IOPscience iopscience.iop.org

Home Search Collections Journals About Contact us My IOPscience

An electro-thermally and laterally driven polysilicon microactuator

This content has been downloaded from IOPscience. Please scroll down to see the full text.

1997 J. Micromech. Microeng. 7 7

(http://iopscience.iop.org/0960-1317/7/1/003)

View the table of contents for this issue, or go to the journal homepage for more

Download details:

IP Address: 140.113.38.11
This content was downloaded on 28/04/2014 at 13:25

Please note that terms and conditions apply.

J. Micromech. Microeng. **7** (1997) 7–13. Printed in the UK PII: S0960-1317(97)76235-1

An electro-thermally and laterally driven polysilicon microactuator

Chi Shiang Pan† and Wensyang Hsu‡§

† Department of Mechanical Engineering, National Chin-Yi Institute of Technology, Taichung, Taiwan, Republic of China
‡ Department of Mechanical Engineering, National Chiao Tung University, Hsin Chu, Taiwan 30050, Republic of China

Received 15 July 1996, accepted for publication 29 October 1996

Abstract. A novel electro-thermally and laterally driven microactuator made of polysilicon has been designed, fabricated, and tested. The operational principle is based on the asymmetrical thermal expansion of the microstructure with different lengths of two beams, but not based on the variable cross sections of the microstructure. A microgripper to demonstrate one possible application of the microactuator is fabricated and characterized. The input voltage of this design is less than 10 dc to produce 20 μm displacement with about 0.6 mJ heat dissipation, and the maximum temperature is less than 600 °C. A gripping force up to 2.8 μN can be generated. Simulation results are compared with the experimental data and show good agreement. Some design parameters strongly influencing the performance of the microactuator are discussed also.

1. Introduction

For the actuation mechanism of microactuators, various techniques such as piezoelectric, thermal–mechanic, magnetic, or electrostatic have been demonstrated. One common use of the thermal–mechanical actuation technique is based on the bimorph effect [1–4], which relies on the difference of thermal expansion coefficients between the components of a sandwiched layer. However such actuators produce deflection in the direction normal to the underlying substrate. For thermally driven microactuators with lateral motion, Guckel *et al* [5] proposed new flexure actuators which can produce motion via the thermal effect and magnetic effect. For the thermal effect, this was based on the asymmetrical thermal expansion of a microstructure with variable cross sections. The variable cross sections resulted in non-homogeneous resistive heating and temperature rises as current was applied. Field *et al* [6] modified Guckel's actuator to design an optical fiber switch with a thermal isolation trench under the hot leg of the actuator. Lerch *et al* [7] used information from Guckel's work to produce a normally closed gripper made by laser micromachining and metal (Ni) electroplating. They studied the characteristics of the thickness of the actuator and the dimensions of the notches.

In this paper, we propose an operational principle and a simple fabrication method to produce an electro-thermally and laterally driven microactuator. The operational principle is based on the asymmetrical thermal expansion of the microstructure with different lengths of two beams, but not based on the variable cross sections of the microstructure. This design principle not only increases the thermal asymmetric effect, but also makes the actuator able to be driven even under the temperature rise of the whole structure. Here, a microgripper to demonstrate one possible application of the microactuator is fabricated and characterized. It is made of polysilicon thick film by a simple surface–bulk micromachining method with only one mask patterned [8–11]. Moreover, the microactuator proposed here is able to be used for microswitch and micropositioning applications, and is also useful for material constant measurements of polysilicon films [5].

§ E-mail: whsu@cc.nctu.edu.tw

2. Concept design

Figure 1 shows the basic concept design of an electro-thermal microactuator. The microactuator consists of a pair of adjacent cantilever beams with different lengths, but the same thermal coefficient to form an actuating arm. The total dimensions of the full structure are within a 1000 μm × 700 μm area, including contact pads. The actuating beams are about 1–3 μm wide and 2–3 μm thick. The length of the longer beam ranges from 500 to 750 μm, and the shorter beam is from 100 to 500 μm, according to different feature size requirements. The main structure of the microactuator is made of undoped polysilicon by low-pressure chemical vapor deposition (LPCVD). Then phosphorus is doped into the top face, which is operated as a conductive layer. Heat generated in the conductive layer causes temperature changes of the actuating arm when current is applied. By the thermal expansion effect, the

0960-1317/97/010007+07$19.50 © 1997 IOP Publishing Ltd

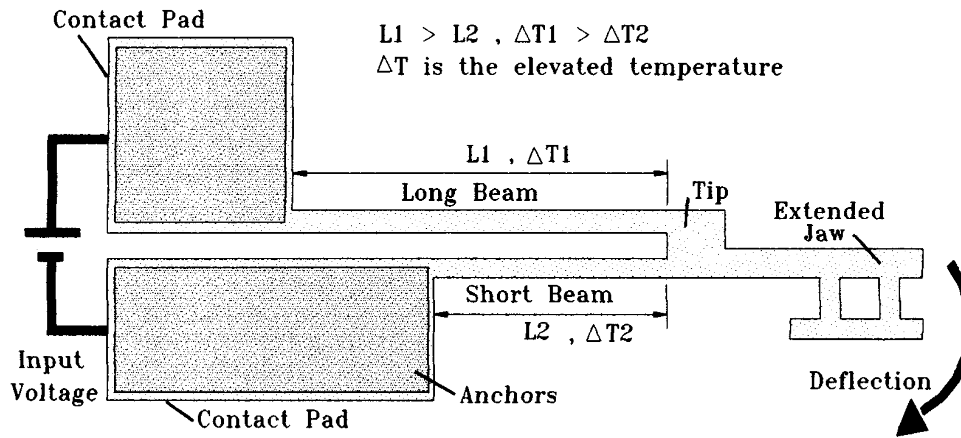

Figure 1. The operating principle of the electro-thermal actuating arm.

Table 1. The related data for the finite-element analysis.

Mechanical properties:		Electric loadings:	
Young's modulus of polySi	150×10^9 Pa	Input dc voltage	$\leq$15 V
Poisson's ratio	0.066	Resistivity	5×10^{-4} Ω m
Density	2320 kg m^{-3}		
Thermal properties		Geometric dimensions	
Conductivity coefficient	41 W m^{-1} °C^{-1}	Gap between beams	$\geq$5 μm
Expansion coefficient	2.7×10^{-6} °C^{-1}	Length of long beam	500–750 μm
Specific coefficient	700 J kg^{-1} °C^{-1}	Length of short beam	100–500 μm
Convection coefficient	50 W m^{-2} °C^{-1}	Width of beams	1–3 μm
Ambient temperature	20 °C	Thickness of beams	2–3 μm
		Thickness of conducting layer	0.5 μm
		Length of extension beam	40–50 μm
		Contact pads	200 μm × 200 μm

long beam elongates more than the short beam. This is not only due to the temperature difference ($\Delta T_1 > \Delta T_2$) between the two beams but also the difference of the lengths ($L_1 > L_2$) between the two beams. Thus, owing to the unequal thermal expansions of two adjacent beams, the two beams curl toward the shorter one.

3. Finite-element modeling (FEM)

Microgrippers are used here to demonstrate the application of our microactuators. The commercial finite-element code ANSYS 5.0a has been used to perform electro-thermo-mechanical analysis. The microgripper is treated as a 3D structure. The meshes are brick shape elements. The steady state temperature distribution of the microgripper, the displacements, and the gripping forces of the jaw under different input voltages are simulated. The fundamental buckling loading and the fundamental frequency of the microgripper are also obtained. In simulation, the material properties which are temperature dependent, such as thermal expansion coefficient, thermal conductivity, resistivity, and Young's modulus [12–14], are treated as constant values here. The related data about the mechanical, thermal, and electric properties of polysilicon, and the dimensions of the microgripper, are listed in table 1.

According to the analysis, we find that heat dissipated through convection, conduction, and radiation to the ambient can be neglected in comparison with the heat losses through conduction to the anchor substrate Si (heat sink), since the thermal conductivity of Si is much larger than ambient air. Figure 2 shows the transient and the steady state temperature distribution of a microgripper under 12 V dc by FEM. It is found that the maximum temperature band shifts and is not located at the jaw region. The experimental result verifies the prediction as shown in figure 3. The temperature along the contact pads appears to be a little higher than ambient temperature. This makes the pads suitable for integration with IC components on the same chip. Figure 2 also verifies that the temperature rise (ΔT_1) along the long beam is higher than the temperature rise (ΔT_2) along the short beam. Figure 4 exhibits the steady state temperatures at the maximum-temperature location of a microgripper under various input voltages. It is observed that the temperature increases nonlinearly as the input voltage increases. The temperature difference between the top and the bottom of the beams will cause a deflection of the beams downward. This results from the transmission of heating power from the top face to the bottom of the beams as current is applied. However the effect is negligible, since the displacement in the

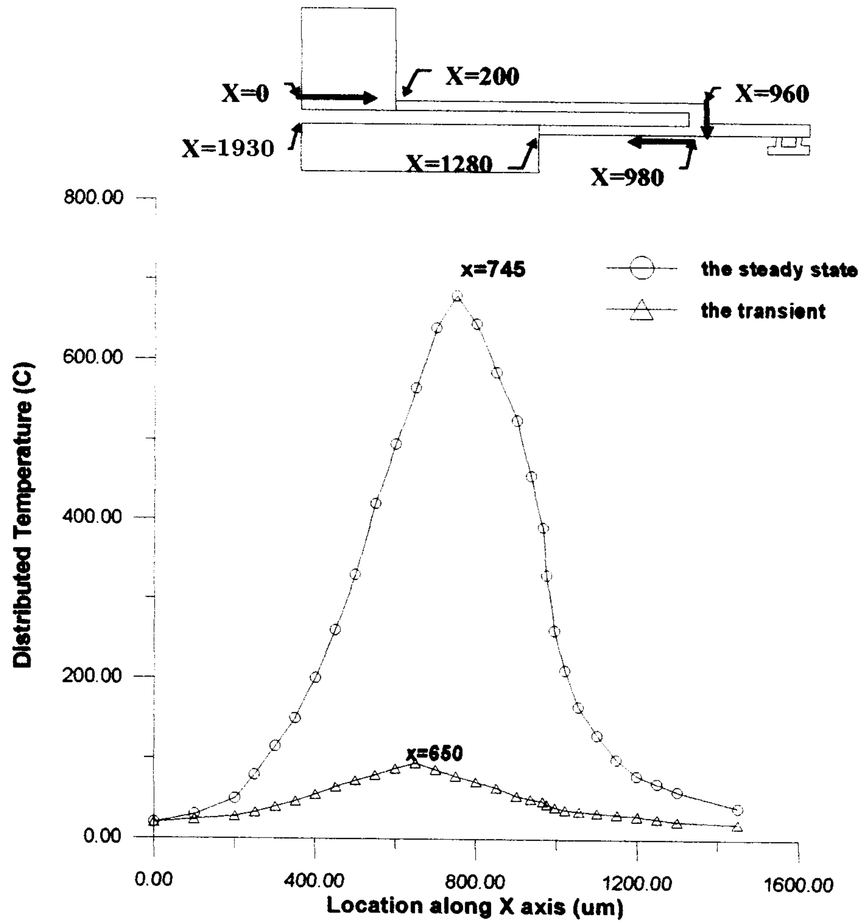

Figure 2. The transient (0.00167 s) and the steady state (0.05 s) temperature distribution of a microgripper under 12 V dc by FEM.

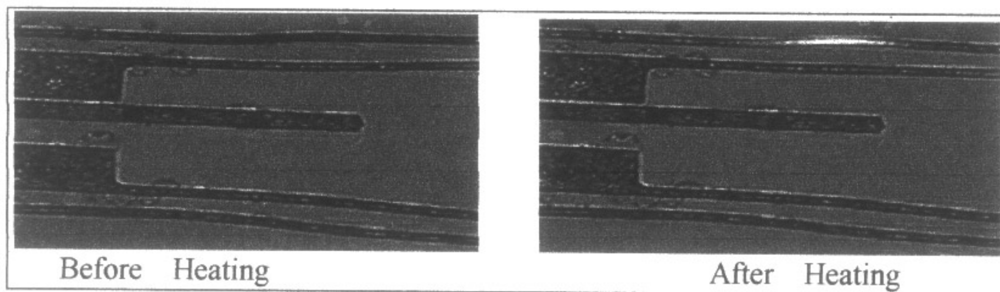

Figure 3. Photographs to verify the location of the maximum temperature (the bright point) of the microgripper.

vertical direction is almost two orders of magnitude smaller than that in the lateral direction. The deflection of the microgripper by its own weight is negligible due to the scale effects [15]. The transient response analysis of the jaw is incorporated into the finite-element model also, as shown in figure 5. It predicts 30 ms to reach steady state with an input voltage of 10 V. After removal of the input voltage, the jaw will recover to its initial state in about 30 ms.

Figure 6 shows the calculated gripping forces versus input voltages. The gripping force is obtained by the following method. It is assumed that a rigid specimen with specified weight is caught between two jaws, and the jaws remain in the initial open state to grip the specimen. The gripping force is just to keep the specimen from slipping down the jaws. The friction coefficient between the jaws and the specimen is assumed to be 0.5 [16] for the calculation.

The fundamental ‘buckling loading (buckling voltage)’ of the microgripper is calculated to be achieved at more than 55 V. The buckling voltage means that the temperature rise under this voltage will cause buckling behavior of

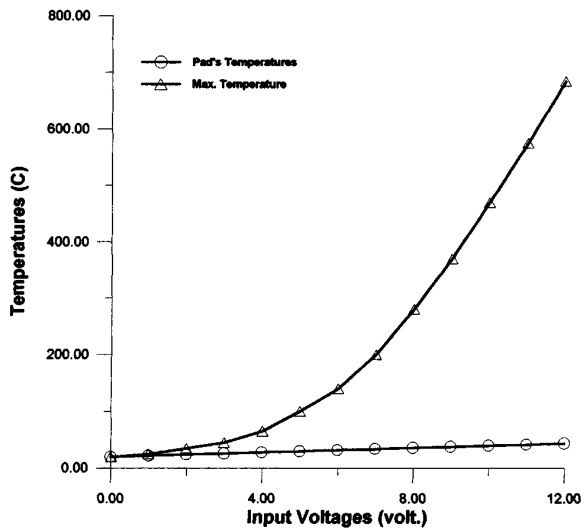

Figure 4. The steady state temperatures of a microgripper under different input voltages by FEM.

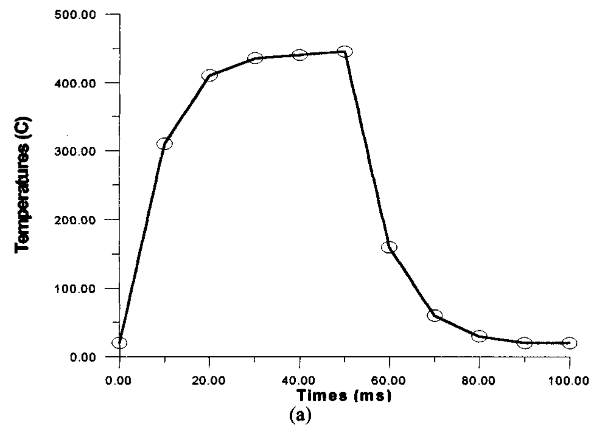

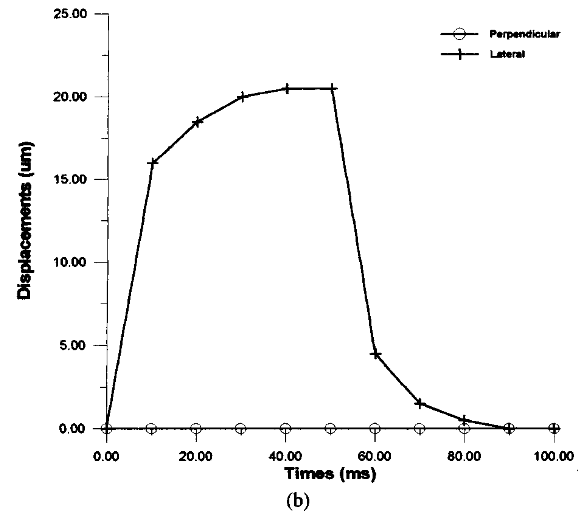

Figure 5. The temperature variations (a), and displacement variations (b) of the jaw for heating 50 ms on then 50 ms off at 10 V input voltage by FEM. (The width and the thickness of the beams are 2 μm, and the lengths of the two beams are 750 and 300 μm. The gap is 6 μm, and the length of the extension jaw is 100 μm).

the structure of the microgripper. However, the voltage is far from the operating voltage and the temperature of polysilicon beams increased by the voltage would reach the melting point of polysilicon before buckling. The fundamental frequency is 43830 Hz, which indicates that we can drive the microgripper by successive pulses below this frequency without serious resonance. The maximum stress corresponding to the microgripper is about 0.05 GPa, which is two orders of magnitude below yield stress.

The influence of the variations of design parameters is also analyzed by FEM to improve the mechanical performance of the microgripper. It is found that the displacement of the jaw is independent of Young's modulus and beam height. Reduction of beam width will increase the displacement a little, and decrease the stress and power consumption a little. The high aspect ratio of the structure shows little improvement in the displacement; nevertheless it makes the microgripper much stiffer in the vertical direction. The relation of the ratio δ/L_1 and L_2/L_1 simulated by FEM is shown in figure 7, where L_1 and L_2 are lengths of the long beam and short beam, respectively, and δ is the displacement of the jaw. It indicates an optimal value of δ/L_1 near $L_2/L_1 = 0.4$ and 0.5 with lengths of the long beam being 750 and 500 μm, respectively. It also shows that increasing the length of the long beam may produce a larger displacement of the jaw. In addition, smaller resistivity of the conductive layer produces the same temperature rise and displacement with a lower input voltage, but it reduces the consumption of the power very little.

4. Fabrication processes

Figure 8 illustrates the process sequences to fabricate the microgripper structure. It is a combination of surface and bulk micromachining technique. First, a (100) wafer is thermally grown with SiO_2 about 0.5 μm thick as a sacrificial layer. Then a 0.3 μm thick LPCVD nitride is deposited to balance the compressive stress of the SiO_2 layer, and for the protection of the microgripper structure during the bulk-etched step. An undoped polysilicon film of 2 μm is deposited by LPCVD. Then the film is subsequently doped with phosphorus. The wafer is spin-coated with photoresist and patterned with a mask which is oriented in such a way that the lengths of the adjacent beams of the actuating arms are in the $\langle 010 \rangle$ direction of the wafer. Then it is immersed in wet etchant to etch the polysilicon. This step defines the structure of the microgripper, as shown in figure 8(b). After stripping photoresist, we can directly position the wafer in H_3PO_4 etchant and then in buffered oxide etchant (BOE) to suspend the actuating arm and the jaws, as shown in figure 8(c). However, the sticking problem may occur easily because of the small space between the suspended structure and the substrate. In order to overcome this problem we skip over step (c) to deposit LPCVD nitride for the protection of the polysilicon structure during the bulk micromachining process. The nitride is then patterned with the same mask in the same manner as in step (b). Subsequently we use the patterned

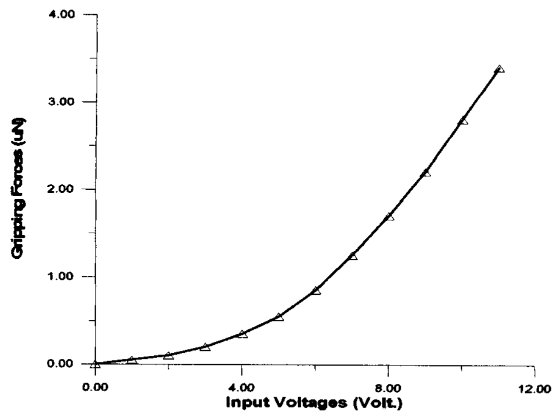

Figure 6. The calculated gripping forces versus input voltages by FEM. (The width and the thickness of the beams are 2 μm, and the lengths of two beams are 750 and 300 μm. The gap is 6 μm, and the length of the extension jaw is 100 μm).

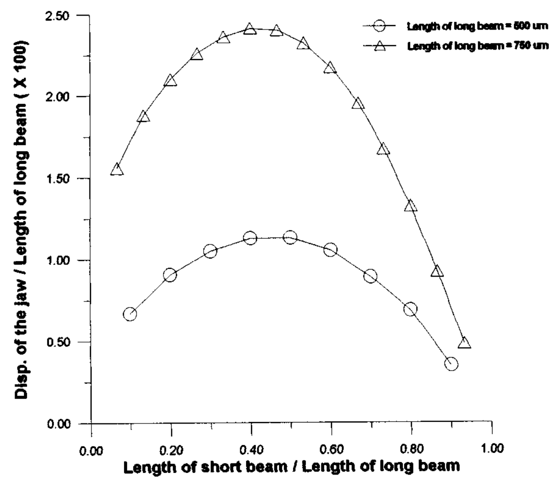

Figure 7. Variations of the dimensionless ration L_2/L_1 versus variations of δ/L_1 by FEM.

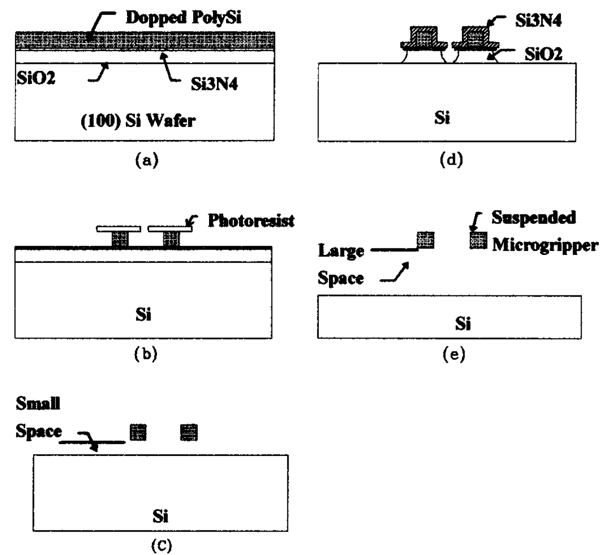

Figure 8. Fabrication process sequences for a microgripper structure.

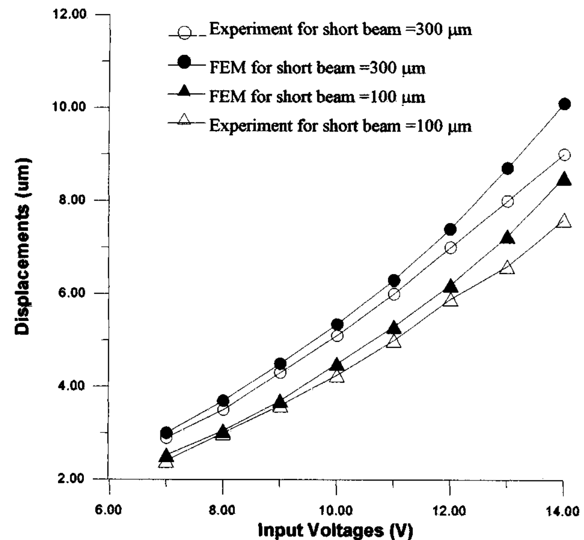

Figure 9. The displacements of the tip of the jaw under different input voltages (the length of the long beam is 500 μm, the lengths of the short beams are 300 and 100 μm, the gap is 7.5 μm, the width and the thickness of the beams are 2.8 and 2 μm; the extension jaw is 40 μm long).

nitride as a mask to etch dioxide, as shown in figure 8(d). Then the wafer is anisotropically time-etched in an alkaline solution, 33 wt% KOH at 85 °C. In such a way, downward etching and lateral etching of silicon directly underneath the passive layer will occur simultaneously in the area where the {100} planes of silicon are exposed [17]. A larger space is simultaneously formed under the actuating arm and the jaw region. In the final step, the passive layer is removed, and the complete microgripper unit is obtained.

5. Experimental results and discussion

To evaluate the deflection of the microgripper, a dc voltage is applied at the contact pads. The displacements of the jaws are measured by an optical microscope ruler mounted on the optical microscope, or by image capture software to capture the pictures from the video. The comparison between experimental results and FEM results is shown in figure 9. We find that the average error is about 8%. Below 9 V, the difference between experimental result and FEM result is about 0.2 μm, but the difference becomes about 1 μm at higher voltages. The reason is that the material properties used in numerical simulation are not completely consistent with the actual properties of the microactuator at high temperature, since the properties of polysilicon at high temperature are unknown. Besides, during the experiment we observed the following phenomenon: when input voltage rises above 15 V, the temperature will approach the melting point of polysilicon, and the beams of the actuating arm become much stiffer. However, this

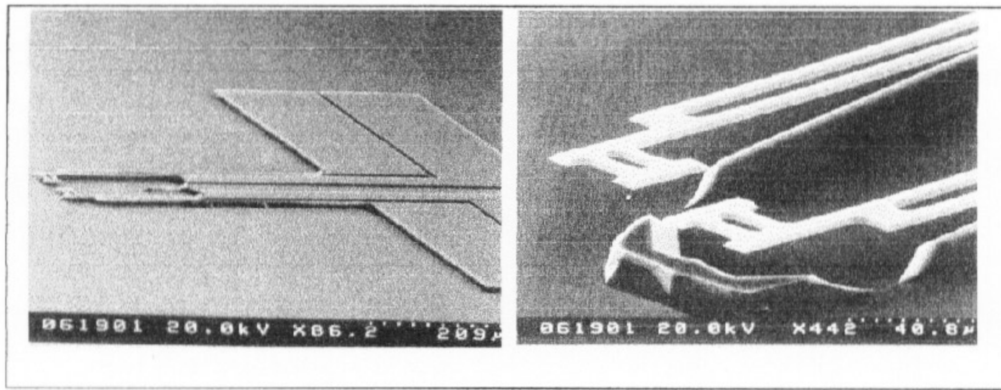

Figure 10. SEM micrographs of a complete microgripper.

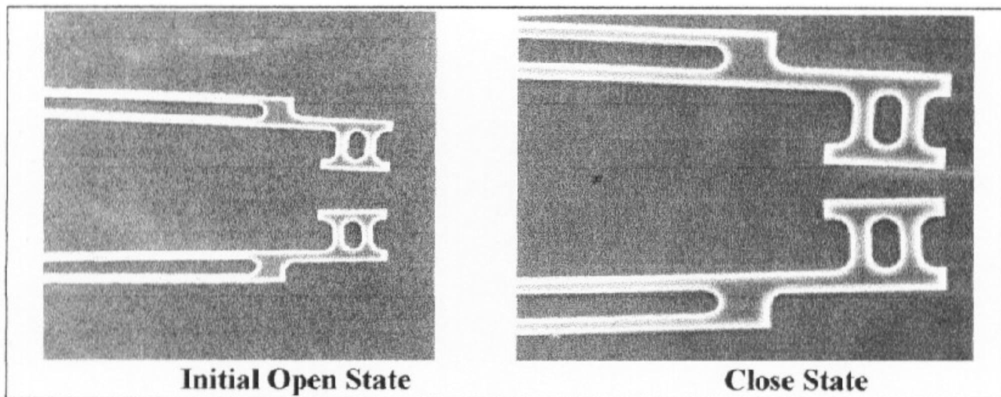

Figure 11. A microphotograph of the deflection of a microgripper.

needs to be further investigated.

It is consistent with prediction that no buckling behavior is observed before the structure is melted at about 1412 °C. The location of the maximum temperature along the beams can be observed in two ways. First we immerse the microgripper in Fluorinet liquid FC43 (3 M company). When the temperature reaches the nucleation temperature, a bubble forms at the location of maximum temperature first [18]. The other way is that when the temperature becomes very high, the location of maximum temperature becomes visually bright. This result confirms the prediction as shown in figure 3. It is not possible to measure the fundamental frequency of the microgripper by observing resonance while tuning the input frequency, since the thermal response always falls behind the input electric signals. The dimensions of the microgripper are measured by SEM after dicing. SEM micrographs of a complete microgripper are shown in figure 10. Finally, a photograph of the deflection of a microgripper is shown in figure 11.

6. Conclusions

Some expected advantages of the microactuator presented in this paper are summarized. (i) A new design principle is proposed. The electro-thermally and laterally driven microactuator exhibits elastic deflection by uneven thermal expansion of two adjacent beams. This is not only due to the temperature difference between the two beams but also the difference of the lengths between the two beams. According to this operational principle, other applications are also possible to construct for various uses, such as microswitches, optical tweezers and micropositioners. (ii) The microgripper fabricated in the paper with a dramatic small feature size has a large working distance and gripping force. The input voltage of this design is less than 10 dc to produce 20 μm displacement with about 0.6 mJ heat dissipation, and the maximum temperature is less than 600 °C. A gripping force up to 2.8 μN can be generated. These performances are significantly improved over microgrippers reported previously with the same feature size. (iii) The fabrication of the structures is defined with only one mask by simple surface and bulk micromachining techniques, which is compatible with IC processes. The temperatures along the contact pads appear to be near the ambient temperature. These advantages make the microactuator suitable for being integrated with IC components on the same chip. (iv) According to the simulation results of the design parameters, the optimal structure of a microactuator can be obtained by varying the lengths of the beams or other parameters.

Acknowledgments

This project was supported by the National Science Council of the Republic of China under grant number NSC85-2215-E009-033. The authors would like to thank the staff at the NCTU Semiconductor Research Centre, and Dr Liwei Lin at the Institute of Applied Mechanics, National Taiwan University, for providing the testing equipment.

References

[1] Riethmuller W and Benecke W 1988 Thermally excited silicon microactuators *IEEE Trans. Electron Dev.* **ED-35** 758–63

[2] Benecke W and Riethmuller W 1989 Applications of silicon-microactuators based on bimorph structures *Proc. IEEE Micro Electro Mechanical System Workshop* pp 116–20

[3] Trah H P, Baumann H, Doring C, Goebel H, Grauer T and Mettner M 1993 Micromachined valve with hydraulically actuated membrane subsequent to a thermoelectrically controlled bimorph cantilever *Sensors Actuators* A **39** 169–76

[4] Buser R A, DeRooij N F, Tischhauser H, Dommann A and Staufert G 1992 Biaxial scanning mirror activated by bimorph structures for medical applications *Sensors Actuators* A **31** 29–34

[5] Guckel H, Klein J, Christenson T, Skrobis K, Landon M and Lovell E G 1992 Thermo-magnetic metal flexure actuators *Technical Digest, IEEE Solid State Sensor and Actuator Workshop (Hilton Head Island, SC)* pp 73–5

[6] Field L A, Burresci D L, Rbrish P R and Ruby R C 1995 Micromachined 1×2 optical fiber switch *Proc. 8th Int. Conf. on Solid State Sensors and Actuators* pp 344–7

[7] Lerch Ph, Kara Slimane C, Romanowicz B and Renaud Ph 1996 Modelization and characterization of asymmetrical thermal micro-actuator *J. Micromech. Microeng.* **6** 134–7

[8] Kim C J, Pisano A P and Muller R S 1992 Silicon-processed overhanging microgrippers *J. Microelectromech. Syst.* **1** 31–6

[9] Chu P B and Pister K S J 1994 Analysis of closed-loop control of parallel-plate electrostatic microgrippers *IEEE Int. Conf. on Robotics and Automation* vol 1, pp 820–5

[10] Suzuki Y 1994 Fabrication and evaluation of flexible microgripper *Japan. J. Appl. Phys.* **33** 2107–12

[11] Sonek G J, Wright W H and Berns M W 1993 Optical tweezers: getting a handle on the microscopic biological world *LEOS '93 Conf. Proc. IEEE Lasers Electro-Opt. Soc. Annu. Meeting* pp 234–45

[12] Okada Y and Tokumaru Y 1984 Precise determination of lattice parameter and thermal expansion coefficient of silicon between 300 K and 1500 K *J. Appl. Phys.* **56** 314–20

[13] Fedder G K and Howe R T 1991 Thermal assembly of polysilicon microstructures *Proc. IEEE Micro Electro Mechanical System Workshop* pp 63–8

[14] Glassbrenner C J and Slack G A 1964 *Phys. Rev.* **134** A1058–69

[15] Pisano A P 1989 Resonant-structure micromotors: historical perspective and analysis *Sensors Actuators* **20** 83–9

[16] Lim M G, Chang J C, Schultz D P, Howe R T and White R M 1990 Polysilicon microstructures to characterize static friction *Proc. IEEE Micro Electro Mechanical System Workshop* pp 82–8

[17] Choi Wia-shing and Smits J G 1993 A method to etch undoped silicon cantilever beams *J. Micro Electro Mech. Syst.* **2** 82–6

[18] Lin Liwei, Pisano A P and Lee A P 1991 Microbubble powered actuator *Proc. IEEE Micro Electro Mechanical System Workshop* pp 1041–4